Experimental Study of the Reaction $^3He(\gamma,\pi^+)^3H$ up to 260 MeV*

J. R. O'FALLON,† L. J. KOESTER, JR., J. H. SMITH,‡ AND A. I. YAVIN
University of Illinois, Urbana, Illinois

(Received 5 August 1965)

The differential cross section for the reaction $^3He(\gamma,\pi^+)^3H$ was measured for photon energies of 180 to 260 MeV. A target of gaseous ^3He at 20.4°K and approximately one atmosphere pressure was irradiated by a 270-MeV bremsstrahlung x-ray beam. The reaction was observed by detecting π^+-^3H coincidences. Tritons with energies between 9.7 and 24.5 MeV (momentum transfer 1.2 F^{-1} to 1.9 F^{-1}) were observed at laboratory angles of 26°, 30°, 35°, and 40°. At 26° the cross sections in the center-of-mass system ranged from 2.55 ± 0.34 μb/sr to 0.78 ± 0.16 μb/sr, decreasing with increasing photon energy. Impulse-approximation calculations relate the cross section to the matter form factor of the 3-nucleon system under the assumption of identical wave functions for ^3He and ^3H. Cross sections found in this experiment lie from 25% to 50% below the values predicted by this theory with form factors from electron-scattering data inserted.

I. INTRODUCTION

THE reaction

$$\gamma+{}^3\mathrm{He}\rightarrow\pi^++{}^3\mathrm{H},$$

which is the subject of this experiment, is particularly attractive for studying pion photoproduction in a complex nucleus. The well defined final state, consisting of a free pion and a triton, permits unambiguous identification of each event in terms of energy and angle or momentum transfer; and it simplifies the interpretation of the cross sections. This cross section can be related through the impulse approximation to an overlap integral of the ^3He and ^3H wave functions. Assuming that ^3He and ^3H can be described by the same wave function,[1] the overlap integral becomes the matter form factor for both ^3He and ^3H. Since this matter form factor can be obtained from the measured ^3He and ^3H charge form factors,[2–4] we can test the application of the impulse approximation to this reaction.

II. EXPERIMENTAL EQUIPMENT AND PROCEDURES

The geometrical arrangement of the equipment is shown in Fig. 1. A 270-MeV bremsstrahlung x-ray beam originated at the betatron target. The beam, after being collimated and cleared of charged particles by a sweeping magnet, was incident upon a ^3He gas target. The ^3He was cooled to liquid-hydrogen temperature at a pressure of 730 mm of Hg. Coincidences were demanded between the photoproduced pions and the recoil tritons. The pion-detector telescope consisted of 7 plastic scintillators; the triton-detector telescope consisted of 4 semiconductor detectors. Both detector telescopes were mounted on carts that rotated independently in a horizontal plane about the target center. The telescope axes intersected at the target center.

Pulses from the detectors were displayed on an oscilloscope and photographed. The heights of these pulses were obtained from the photographs and used for particle identification and, in the case of the triton telescope, energy determination. Triton energies from 9.7 to 24.5 MeV (corresponding to momentum transfers

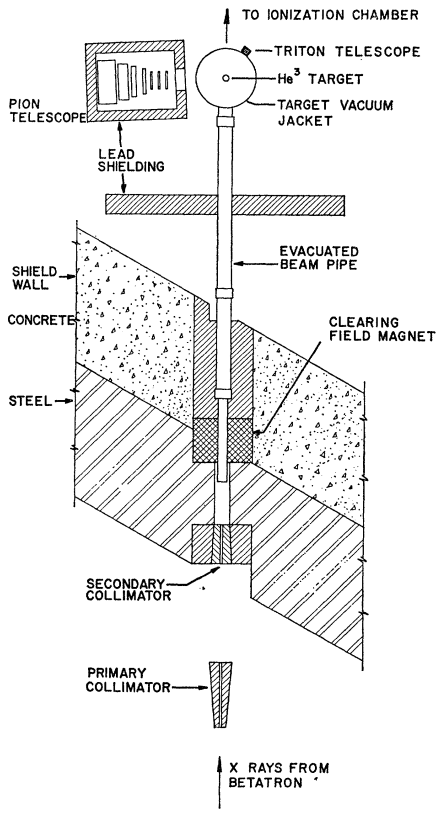

FIG. 1. Geometrical arrangement of the experiment.

* This work was supported in part by the U. S. Office of Naval Research and the National Science Foundation.

† Present address: Department of Physics, University of Michigan, Ann Arbor, Michigan.

‡ On sabbatical leave 1965–66 at Deutsches Elektronen Synchrotron (DESY), Hamburg, Germany.

[1] R. G. Sachs, *Nuclear Theory* (Addison-Wesley Publishing Company, Inc., Reading, Massachusetts, 1953), pp. 180–190.

[2] H. Collard and R. Hofstadter, Phys. Rev. **131**, 416 (1963).

[3] H. Collard, R. Hofstadter, A. Johansson, R. Parks, M. Ryneveld, A. Walker, M. R. Yearian, R. B. Day, and R. T. Wagner, Phys. Rev. Letters **11**, 132 (1963).

[4] H. Collard, R. Hofstadter, E. Hughes, A. Johansson, M. Yearian, R. Day, and R. Wagner, Phys. Rev. **138**, B57 (1965).

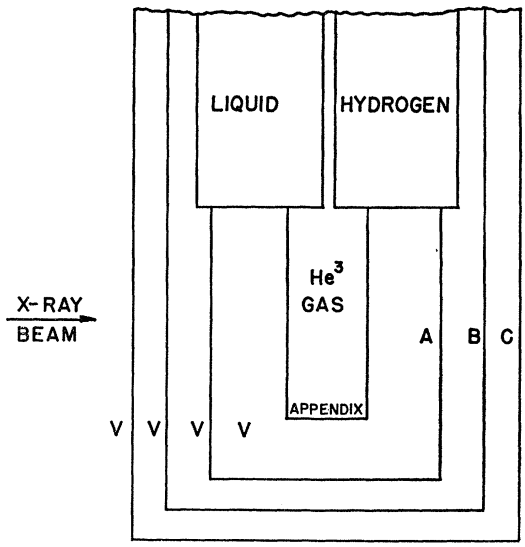

FIG. 2. Schematic representation of the target assembly showing the relation of the gas target (appendix) to the liquid hydrogen reservoir. Regions marked V are evacuated. Radiation shields A and C are in thermal contact with the liquid-hydrogen and liquid-nitrogen reservoir, respectively; B is a floating shield.

of 1.2 to 1.9 F^{-1}) were measured at laboratory angles of 26°, 30°, 35°, and 40° with the pion telescope at the median angles demanded by kinematics: 111°, 100°, 92.5°, and 77.5°, respectively.

The pion telescope was not large enough to intercept the pion correlated with every triton that registered in the triton telescope. Requiring a coincidence thus reduced the counting rate, but it increased the certainty of the identification of events corresponding to the reaction $^3He(\gamma,\pi^+)^3H$. A calculation of the coincident geometrical efficiency was performed by a Monte Carlo method with a digital computer (see Sec. IV).

A. The Bremsstrahlung Beam

The bremsstrahlung x-ray beam from the betatron was collimated by a lead primary collimator 33.7 cm long with a rectangular entrance hole 0.788 cm high by 0.394 cm wide. This gave an x-ray beam 3.57 cm high by 1.83 cm wide at the target. The primary collimator, located 1.20 m from the betatron target, was followed by a secondary collimator 2.05 m from the betatron target. The opening in the secondary collimator was large enough to clear the main x-ray beam, but secondary radiation produced in the primary collimator was absorbed. After leaving the secondary collimator, the beam passed through a clearing field magnet capable of removing 300-MeV electrons from the beam. It then entered an evacuated beam pipe which led to the ^3He target approximately 4.6 m from the betatron target. The experimental area was shielded from the betatron by approximately two feet of steel and two feet of concrete.

Downstream from the ^3He target, the total energy in the beam was monitored by an ionization chamber which was calibrated immediately prior to this experiment. The accuracy of the calibration at a betatron energy of 260 MeV was $\pm 2.3\%$.[5]

The betatron was operated at two energies during the course of the experiment, 260 and 270 MeV. Energy calibration of the betatron was carried out by the engineering staff 18 months prior to this experiment. The energy of the accelerated electrons was known within 0.25%.[6] The width of the x-ray pulses, typically 175 μsec, introduced a spread of approximately $\pm 1\%$ in the peak energy of the x-ray spectrum.

B. The Target

The target is similar to the one described by Whalin and Reitz.[7] The essential part, called the appendix, is a 2.86 cm-diam cylindrical container made of 0.0015 in. Mylar which held the gaseous ^3He target material in thermal contact with a reservoir of liquid hydrogen. This is similar to the appendix designed for use with liquids by Nicolai.[8] Figure 2 shows the relation of the appendix to the liquid-hydrogen reservoir.

At the conclusion of the experiment a test was conducted to determine whether or not the gas in the appendix was at liquid hydrogen temperature. With the complete target assembly at room temperature, the appendix and associated gauges and tubing were filled with ^4He to a pressure of 750 mm of Hg. The system was then sealed off, and the target assembly was cooled in the same manner as for the main experiment. The final temperature was calculated using the ideal gas law. The result was 21°K with an estimated accuracy of $\pm 5\%$. This is consistent with the temperature of boiling liquid hydrogen, 20.4°K. Subsequently, for a different experiment, a similar appendix was prepared with a carbon

TABLE I. Dimensions of pion telescope.

Scintillator	Vertical height (cm)	Horizontal width (cm)	Thickness (cm)	Distance to target center (cm)	Pion energy to reach scintillator (MeV)
$\pi C1$	9.54	8.93	0.641	31.0	3.2
$\pi 1$	9.52	8.93	0.643	34.8	11.2
$\pi C2$	9.52	8.87	0.637	38.6	16.0
$\pi 2$	12.70	13.34	1.33	42.1	19.8
$\pi 3$	14.90	15.55	2.57	46.9	25.6
$\pi 4$	17.85	18.45	5.05	51.1	37.0
$\pi 5$	22.2	22.8	8.82	57.1	54.0

[5] W. P. Swanson, Physics Research Laboratory Internal Report, University of Illinois, 1963 (unpublished).
[6] R. Wallstrom, J. Stahlke, and L. Rogers, Physics Research Laboratory Internal Report, University of Illinois, 1962 (unpublished).
[7] E. A. Whalin, Jr., and R. A. Reitz, Rev. Sci. Instr. **26**, 59 (1955).
[8] V. O. Nicolai, Rev. Sci. Instr. **26**, 1203 (1955).

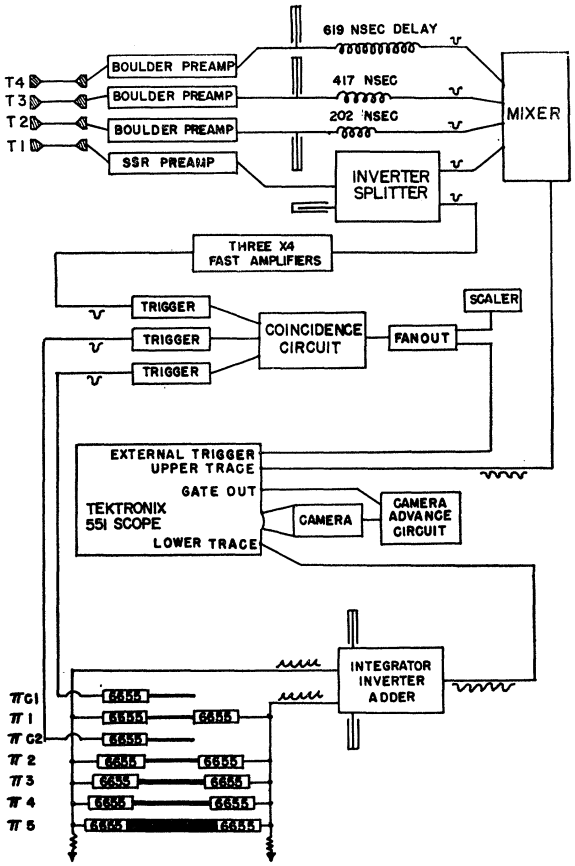

FIG. 3. Block diagram of the logic and pulse display circuitry.

resistance thermometer imbedded in the bottom.[9] The thermometer was calibrated by filling the appendix with liquid ^{4}He. When the liquid was removed and the appendix was filled with gaseous ^{3}He cooled by liquid ^{4}He, the thermometer read within 1% of its liquid helium calibration. We believe this temperature is accurate to 2%, and the uncertainty has been ignored in subsequent calculations. Therefore, 20.4°K has been used as the temperature of the gaseous ^{3}He.

C. Detector Telescopes

The pion detector telescope was similar to that described by Walker, Smith, and Koester.[10] It consisted of seven rectangular plastic scintillators (Nuclear Enterprises 102), labeled $\pi C1$, $\pi 1$, $\pi C2$, $\pi 2$, $\pi 3$, $\pi 4$, and $\pi 5$, in the order of their distances from the target. Counters $\pi C1$ and $\pi C2$ were each viewed by one RCA 6655A photomultiplier tube and were used to make coincidences. Pulses from the remaining scintillators were viewed by two such tubes each and were used for particle identification and energy determination. The dimensions of the pion telescope are listed in Table I. The telescope was tapered out to prevent loss of pions by Coulomb scattering. Scintillator $\pi C2$ defined the solid angle of the pion telescope.

The triton-detector telescope consisted of four transmission-type surface-barrier silicon semiconductor detectors (Oak Ridge Technical Enterprises Corporation, model No. TMHJ300). The four detectors, labeled $T1$, $T2$, $T3$, and $T4$, were circular with a surface area of 3 sq cm. Adjacent detectors were separated by $\frac{5}{16}$ in. The range-energy characteristics of the triton telescope are listed in Table II. The first detector, $T1$, which provided a coincidence signal with $\pi C1$ and $\pi C2$, was 17.2 cm from the center of the target.

The solid-state detectors were designed to be used totally depleted, so that all the energy lost by a charged particle in traversing the detector would contribute to the output signal. Dead layers in the front of each detector, as measured by the manufacturer, corresponded to an energy loss of approximately 7 keV by a 5.5-MeV alpha and therefore were neglected. Since the depletion depth is proportional to the square root of the voltage applied across the detector, there is a voltage below which the depletion layer does not extend through the detector. We found that in order to keep the reverse currents at safe levels the bias voltages on detectors $T2$, $T3$, and $T4$ had to be reduced below this value. Thus these detectors were not totally depleted, and dead layers existed on the back sides of the detectors. The dead layer thicknesses for $T2$ and $T3$, determined by relating the maximum observed pulse heights to the sensitive thicknesses by means of range-energy relations, were 12.5% and 43%, respectively, of their total thicknesses. Since most of the tritons stopped in $T1$ and $T2$ and none reached $T4$, these dead layers did not present a serious problem. The energy bins were selected to include in one energy bin all tritons that stopped in a given dead layer. Thus the energy assignment for tritons stopping in a dead layer, which was less certain than for other tritons, introduced no uncertainty into the experimental cross section.

D. Electronics

Events corresponding to the reaction $^3He(\gamma,\pi^+)^3H$ were detected by means of the coincident charged particles passing through the counter telescopes. The energy lost by a particle in traversing each detector was

TABLE II. Characteristics of triton telescope.

Detector	Thickness (microns)	Triton energy to reach the detector (MeV)
$T1$	388	7.2
$T2$	515	14.2
$T3$	940	20.8
$T4$	345	30.3

[9] N. M. O'Fallon (private communication).
[10] A. B. C. Walker, J. H. Smith, and L. J. Koester, Technical Report No. 41, Contract ONR 1834(05), Physics Research Laboratory, University of Illinois, 1962 (unpublished).

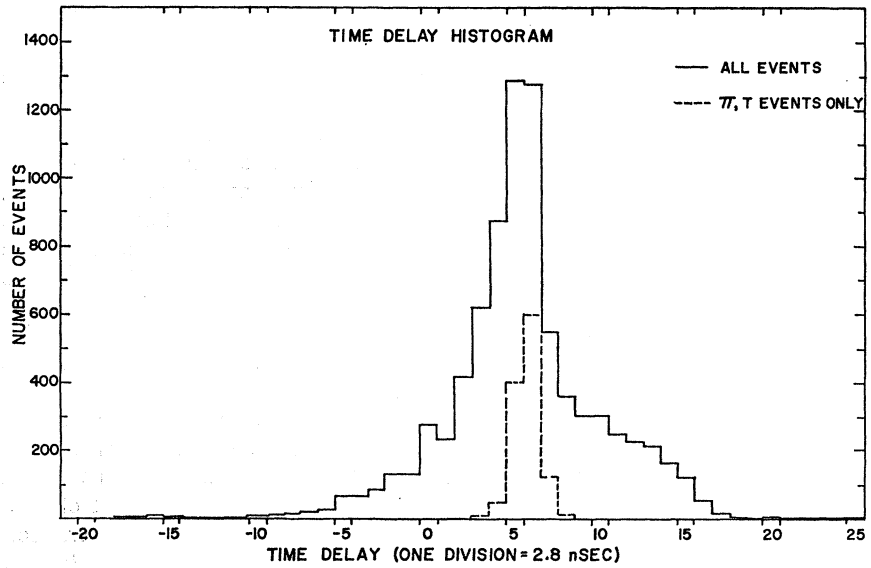

FIG. 4. Histogram of the time delay between the first pion pulse and the first triton pulse as measured on the oscilloscope traces.

measured by the pulse height displayed on a calibrated dual beam oscilloscope (Tektronix 551). Photographs of these pulses constituted the data of the experiment.

The methods used to obtain these pulses and to trigger the oscilloscope will now be described. A block diagram of the data collection and logic circuits is shown in Fig. 3. Scintillators $\pi 1$, $\pi 2$, $\pi 3$, $\pi 4$, and $\pi 5$ of the pion telescope were viewed by pairs of RCA 6655A photomultiplier tubes. Pulses from the dynodes of the phototubes on one side of the detector telescope entered an RG 62/U coaxial cable at intervals of 22.5 m (90 nsec) through circuits which made the transmission line appear unbroken to signals already on the line.[10] When a signal entered the line, it split, half going in each direction. One end of the line was terminated; the other end, along with a similar line connected to the dynodes of phototubes on the other side of the telescope, went to a circuit where the two pulse trains were added, integrated, and inverted. The resultant pulses were displayed on the lower trace of the dual beam oscilloscope.

Signals from the four semiconductor detectors of the triton telescope were amplified by fast preamplifiers whose rise times were 3 nsec for the $T1$ preamplifier (Solid State Radiations, Inc., model 107) and 8 nsec for the other preamplifiers (Boulder Nuclear Instruments, model N-10A). The amplifier outputs were clipped to a length of 43 nsec, delayed by successively longer times, fed through a mixer circuit, and displayed on the upper trace of the dual beam oscilloscope. Since the output signal from the preamplifier on $T1$ was positive while the other three were negative, its signal was inverted and split before going into the mixer. The other part of the split signal was used in the logic. The modular logic circuits had been developed in the electronics laboratory of the high-energy physics group at the University of Illinois.

The oscilloscope was triggered in the following way. Three signals, $\pi C1$ and $\pi C2$ from the pion telescope and $T1$ from the triton telescope, were standardized by discriminator circuits which produced logic pulses of predetermined lengths: 16 nsec for the pion telescope and 26 nsec for the triton telescope. These three pulses went into a 3-fold coincidence circuit whose output triggered the oscilloscope and activated a scaler. Thus, whenever two charged particles entered the two detector telescopes within approximately 20 nsec of each other and lost enough energy to fire the discriminators, the oscilloscope was triggered. The oscilloscope traces were photographed by a Bell and Howell Model D animation camera on Kodak Linograph Ortho film. The shutter was open at all times, and the film was advanced after each event by an external gate signal from the oscilloscope.

E. Experimental Procedures

In order that no pion-triton coincidences be lost, two requirements must be met by the electronics: (1) the three logic pulses must be in proper coincidence, and (2) the threshold levels of the three discriminator circuits must be low enough to trigger on all pulses of interest. This section describes how these conditions were obtained.

The timing of the coincidence between $\pi C1$ and $\pi C2$ was performed in the standard manner.[11] This resulted in a broad, flat counting plateau about 28 nsec wide with a decrease to a 3% accidental background in about 5 nsec.

After $\pi C1$ and $\pi C2$ were placed in coincidence, $T1$ was timed with respect to the pion counter. This was difficult to do with two-particle coincidences because

[11] For details, see J. R. O'Fallon, Ph.D. thesis, Physics Research Laboratory, University of Illinois, 1965 (unpublished).

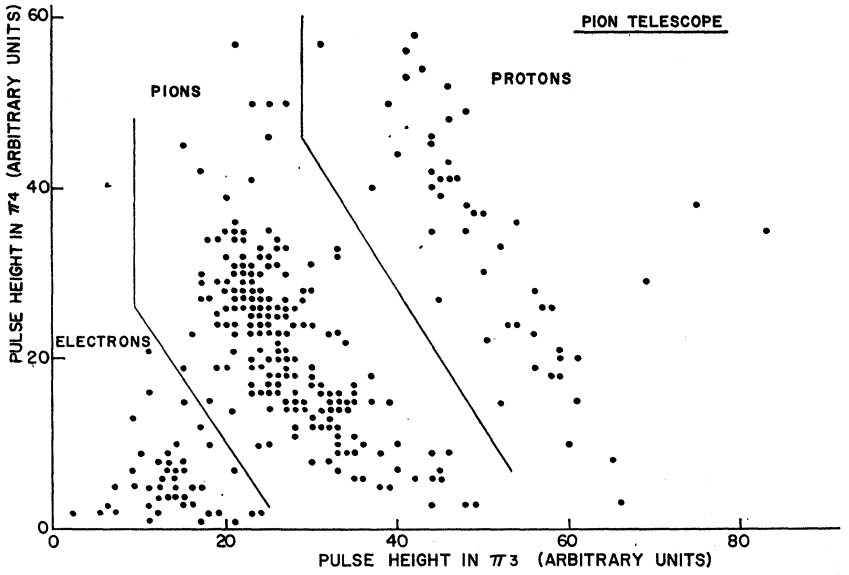

FIG. 5. Typical identification graph for particles stopping in counter $\pi 4$ of the pion telescope. Similar graphs were used to identify particles stopping in $\pi 2$, $\pi 3$, and $\pi 5$.

the counting rate was too low. Therefore, $T1$ was removed from its telescope and placed directly in front of the pion counter. With this arrangement, the high flux of charged particles going through $T1$ and the pion telescope could be used for timing. Most of such particles were minimum ionizing and were not counted with 100% efficiency by the thin semiconductor detector. Consequently, a broad sharply defined plateau in the counting curve could not be obtained; however, a plateau was evident. We then delayed the pion signal by an amount calculated to place it in coincidence with the signal from the rather slow tritons. Time resolution was kept broad enough to allow for the spread in flight time for the various energies. When the pulse heights were read from the film, the time delay between the particles in the two telescopes was also directly measured. Figure 4 shows a histogram of those time delays and provides convincing evidence that the pion and triton telescopes were in proper time coincidence. Pion-triton events are seen to be sharply correlated in time with the peak located in the middle of the rather broad time acceptance of the coincidence circuit.

The simplest procedure for assuring triggering on all pions would have been to have set the pulse-height discriminator level on $\pi C1$ and $\pi C2$ low enough to count all minimum ionizing particles. This resulted in too great an accidental background of coincidences. Therefore the level selectors were set just low enough to trigger reliably on the fastest pions needed for this experiment. An auxiliary triggering system was arranged to photograph all particles which got at least as far as $\pi 5$, even for $\pi C1$ and $\pi C2$ pulses which were below minimum ionizing levels; i.e., the auxiliary system was set to trigger on everything which reached $\pi 5$. Included on the photograph of the pulses for each event was a signal which indicated that the regular $\pi C1$ and $\pi C2$ coincidence had fired. These photographs were scanned to ensure that all pions had fired the $\pi C1$ and $\pi C2$ coincidence.

Calculation shows that the smallest pulse of interest in $T1$ represents the 4 MeV lost by a stopping triton at the lower limit of Bin 1. α particles from ^{241}Am were passed through foils to give a 3.5 MeV pulse in T1 that was used to set the discriminator level. When the discriminator level is set low enough to trigger on these alpha particles it will also trigger on all tritons of interest. To avoid rise time delays on the pulses, the discriminator was set at one half that required by the alpha particles.

III. DATA ANALYSIS

The triton telescope signals were used, after both particles were identified, to determine the kinematics of each event. For cross sections, the events were collected in five intervals of triton energy which will be discussed below. The first two intervals included essentially those tritons which stopped in $T1$, the third and fourth include those which stopped or almost stopped in $T2$, and the fifth includes those which stopped in $T3$. Since $T4$ could not be reached by the tritons, it served mainly as a check on the ranges. The pion telescope played an important role in identifying the events.

A. Particle Identification

The photographs of the pulses were projected with enough magnification so that the largest pulse heights could be measured with a precision of about 1%. Pions were identified by means of graphs like the one in Fig. 5. Each event was plotted as a point with coordinates representing the pulse heights in the last two detectors reached by the particle, e.g., $\pi 3$ and $\pi 4$ in Fig. 5. Particles of equal mass lie on the same locus so that electrons, pions, and protons are identifiable. The pulse

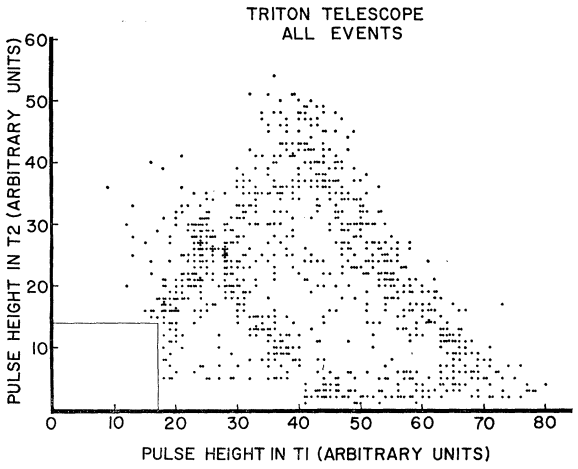

FIG. 6. Identification graph for particles stopping in $T2$ of the triton telescope. This figure includes all coincidence events regardless of type of the particle in the pion telescope. The blank box is densely populated with electrons not shown. The bands of points with slope approximately -1 represent protons, deuterons (rather sparse), and tritons, with the heaviest particles lying farthest from the origin. A reading cutoff eliminates events with $T1 \leq 40$, $T2 \leq 4$.

heights in the preceding counters are helpful in resolving doubtful cases. Those pions, for example, which produced nuclear interactions in the scintillator material could usually be recognized as pions by their first few signals when their last two did not lie near any mass locus.

The tritons that stopped in $T2$ or $T3$ were identified from graphs like that in Fig. 6. This graph together with the one in Fig. 7 illustrates the advantage of observing both particles. Figure 6 contains all particles (heavier than pions) that stopped in $T2$, whereas Fig. 7 includes only those that were correlated with pions in the pion telescope. The proton-pion and deuteron-pion coincidences are clearly distinguishable on this plot. Most of the nontriton-nonpion events in Fig. 6 are accidental coincidences with poor time correlation on the photographs (see Fig. 4).

A somewhat different problem is indicated by the points enclosed by the dotted line box in Fig. 7. Most of these events should not have appeared in $T2$. The triton stopped in $T1$, while a stray particle, probably an electron, happened to strike $T2$ at the same time. The random rate of arrival of such small pulses as these was consistent with the number of accidental coincidences enclosed in the box in Fig. 7. When one piled up on another pulse, the shape was changed enough so that its effect could be subtracted in the pulse-height measurement. A real difficulty would arise in determining which of the points at the lower right corner of Fig. 7 truly represented tritons stopping in $T2$ and which came from tritons stopping in $T1$ with a small accidental pulse in $T2$. This difficulty was avoided by choosing the boundaries of the energy interval to straddle this uncertain region. The same procedure was applied for tritons stopping near the front surfaces of $T3$ and $T4$.

Tritons which stopped in $T1$ could not be distinguished from protons or deuterons unless they gave up more energy than was possible for either of those particles. The lowest energy interval (Bin 1) contained pulse heights in $T1$ that could have been produced by protons or deuterons, but not by electrons except under very unusual circumstances. Bin 2 pulses could have been produced only by deuterons or tritons. The amount of contamination was estimated by finding, from graphs like Fig. 7, the number of proton-pion and deuteron-pion coincidences per MeV for each angle. These numbers appeared to be constants independent of energy, so that the proton subtraction varied between $(6\pm3)\%$ and $(12\pm4)\%$ for Bin 1 and the deuteron subtraction between $(1\pm1)\%$ and $(7\pm3)\%$ in Bins 1 and 2 (see Table IV). The difference in energy dependence between these backgrounds and the tritons was not surprising because the triton recoils were profoundly influenced by a form factor.

B. Energy Calibration

The semiconductor detectors were calibrated at the end of the experiment by depositing a small amount of ^{212}Pb from the ^{232}Th radioactive series on the face of each detector. This radioactive source emits two discrete alpha lines of 6.05 and 8.78 MeV. The corresponding pulses were displayed on the oscilloscope, photographed, and measured in the same manner as the regular data. This provided two points on the energy-versus-pulse height graph, in addition to the one at the origin, for each detector. The amplifier linearity from the semiconductor output through the oscilloscope was checked with a calibrated pulser which produced an output pulse shaped like that from the detectors. All systems were linear, so a best-fit straight line represented by the equation $P=K_iE$ was drawn through the three points

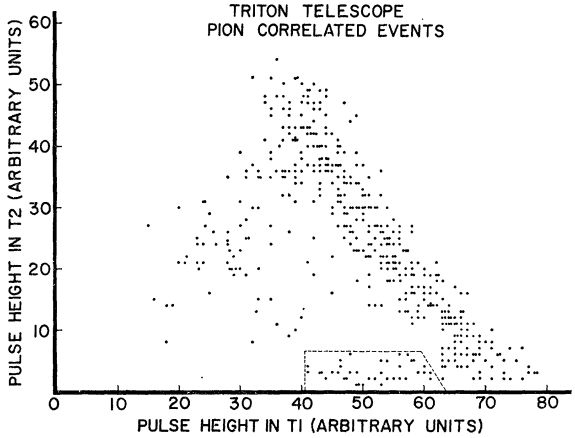

FIG. 7. Those events from Fig. 6 which are in coincidence with pions.

for each detector calibration. Here P was the pulse height resulting from an energy loss E in the detector, and K_i was the proportionality constant for the ith detector.

These detector calibrations together with range-energy relations were used to calculate the curve of pulse height in $T2$ versus pulse height in $T1$. The calculated curve fell somewhat on the high side of the data points of Fig. 7. In an effort to explain the disagreement, we made some calculations based on known properties of semiconductors. The first calculation involved the charge collection time.[12,13] Since (a) the hole mobilities are some three times smaller than electron mobilities, (b) the holes were collected at the front surface of these detectors, and (c) we had to clip the output signal to 43 nsec to avoid pileup, we feared that the hole transit time for tritons that reached the back surface might be longer than the pulse duration. Actually, we were able to see a change in rise time for particles that traversed the full thickness, but still the rise time seemed less than the pulse duration. The result of this calculation was that the largest pulses could be affected, but the over-all fit to the data points would not be much improved.

The second property considered was the channeling of particles through the crystalline lattice along certain directions with anomalously small energy loss by ionization.[14,15] Since most of the published measurements of this phenomenon were carried out with collimated beams of low-energy particles traversing thin crystals (10–100 μ thick), it was difficult to estimate the magnitude of this effect on the uncollimated tritons penetrating the 388-μ thickness of $T1$. The geometry was such that fewer than 10% of the tritons could enter $T1$ within a cone of 1° half angle about the axis. We concluded that the general spreading of points in Fig. 7, with gaps between the proton, deuteron, and triton loci, could not be explained simply in terms of anomalous energy losses.

Although the disagreement between the calculated curve and the data of Fig. 7 was not satisfactorily explained, rather slight changes in the K_i of the energy calibrations brought the calculated curve to the center of the band of data points. The changes in K_1 and K_2 were -2.8% and -5.8%, respectively. The sensitivity of the fit to the data indicated a rather small uncertainty in the determination of K_1 and K_2, about $\pm 2\%$. This curve-fitting method was used exclusively to determine K_3 with an estimated error of $\pm 5\%$, since the connector broke loose during the radioactivity calibration of $T3$. In any case, the energy calibration of $T3$ was the least important because all tritons stopping in $T3$ were lumped into the highest energy interval (Bin 5) except those which stopped very near the front surface (Bin 4). These triton energies thus were determined primarily by range. The triton energy intervals corresponding to Bins 1–5 are given in Table III.

TABLE III. Energy-bin limits.

Bin No.	Interval of triton energies at target center (MeV)
1	8.6–10.7
2	10.7–14.6
3	14.6–16.5
4	16.5–21.9
5	21.9–30.3

C. Data Corrections

In addition to the correction already mentioned for pion-correlated protons and deuterons stopping in $T1$, corrections must be made for the geometry of the semiconductor telescope, for pion scattering and decay in the scintillators, and for the frames with double traces superimposed. The background of accidental pion-triton coincidences was negligibly small, as indicated by Fig. 4.

In order to measure the empty target background, the ^3He gas was pumped out to a residual pressure of 2 mm Hg (by means of a Toepler pump). Normal operating pressure was about 730 mm Hg. During a total irradiation of 546 J as compared with 6770 J used for the main data, only one pion-triton coincidence was observed from the empty target. The expected result was 0.3 event for this amount of irradiation at this residual pressure of ^3He. Apparently, the wall contribution was negligible.

A brass post in the target assembly, which had to be moved with every change in angle, was inadvertently left in place when the pion telescope was moved to 100°. About 67% of the data at this angle were taken with the post shadowing part of the pion telescope from some points in the target. A Monte Carlo small-angle multiple-scattering correction was made to these data. Cross sections obtained from the corrected data agreed with those obtained from data collected at this angle with the post removed.

The corrections for pion scattering and decay in the scintillator telescope were not so severe as in the well known method of a final counter with inert stopping material in front of it. The pions here registered incrementally as long as they remained in the telescope. A correction based on experimental cross sections for pion-proton scattering and for scattering and absorption

[12] H. M. Mann, J. W. Haslett, and G. P. Lietz, IRE Trans. Nucl. Sci. NS-8, 151 (1961).
[13] P. A. Tove and K. Falk, Nucl. Instr. Methods 29, 66 (1964).
[14] C. Erginsoy, H. E. Wegner, and W. M. Gibson, Phys. Rev. Letters 13, 530 (1964).
[15] A. R. Sattler and G. Dearnaley, Phys. Rev. Letters 15, 59 (1965). This paper contains a bibliography.

TABLE IV. Summary of data and corrections of data.

Telescope settings in lab θ_T, θ_π	Energy bin No.	No. of events (uncorrected)	Triton telescope geometrical correction[a] I	II	III	Proton background	Deuteron background	Pion scattering	Pion decay	Double trace frames	No. of events (corrected)
26°, 111°	1	74	···	−1.7	−4.9	−7.7	−5.0	+1.0	0.0	+1.1	56.8
	2	91	···	···	−3.6	···	−4.2	+2.2	+1.9	+1.8	89.1
	3	38	−1.1	···	E.P.	···	···	+1.5	+0.6	+0.8	39.8
	4	55	−0.8	···	E.P.	···	···	+2.8	+0.8	+1.2	59.0
	5	21	E.P.	E.P.	···	···	···	+1.1	+0.2	+0.4	22.7
30°, 100°	1	89	···	−0.6	−4.2	−11.1	−5.0	+1.6	+1.7	+1.3	72.7
	2	104	···	···	−3.8	···	−4.2	+3.5	+1.6	+1.8	102.9
	3	38	−0.3	···	E.P.	···	···	+1.8	+0.7	+0.7	40.9
	4	48	−0.3	···	E.P.	···	···	+2.3	+0.6	+0.9	51.5
35°, 92.5°	1	91	···	0.0	−4.6	−5.5	−0.8	+3.0	0.0	+1.6	84.7
	2	131	···	···	−4.9	···	−0.7	+6.0	+2.0	+2.5	135.9
	3	55	0.0	···	E.P.	···	···	+3.0	+0.5	+1.1	59.6
	4	51	0.0	···	E.P.	···	···	+2.6	+0.5	+1.0	55.1
40°, 77.5°	1	134	···	0.0	−1.6	−14.4	−2.5	+5.9	+1.9	+2.8	126.1
	2	128	···	···	−3.6	···	−2.1	+6.7	+1.2	+2.9	133.1
	3	36	0.0	···	E.P.	···	···	+1.9	+0.3	+0.9	39.1

[a] I corrects for tritons that went through $T1$ and $T2$ but missed $T3$. II corrects for tritons that went through $T1$ but missed $T2$ and $T3$. III corrects for tritons that went through $T1$ but missed $T2$. E. P. means the correction was made by the efficiency program.

by carbon[16–21] (the two constituents of the scintillators) was made by calculating the fraction of pions removed from the telescope by scattering or absorption before they could be identified as pions. Depending on energy and angle, this correction[11] varied between $(2\pm1)\%$ and $(5\pm1)\%$.

A π-μ decay was of no consequence if the muon stayed in the telescope, since it looked like a pion. A graphical method[11] based on simplifying geometrical assumptions indicated that up to 2.3% of the pions, again depending on energy and angle, decayed into muons such that the event went undetected.

In 2% of the pictures taken, two pairs of traces appeared on the same frame. Since in most of these cases the pairing of the pion pulses with the triton pulses was ambiguous, no attempt was made to use these frames, and the data were corrected accordingly. This correction was labeled "double trace frames" and included with the others in Table IV.

Since the semiconductor detectors all had the same surface area but were successively farther from the target, a geometrical correction had to be made for the decreasing solid angle. The over-all result of this correction was to transfer some events from the lower energy bins to higher ones. An efficiency program discussed below automatically computed the proper solid angle for each energy bin, but the subtraction from the lower bins was done by hand.[11]

Table IV summarizes the data and the corrections. The numbers refer to actual numbers of events recorded at each angular setting and grouped according to the triton laboratory energy.

IV. EVALUATION OF CROSS SECTIONS

Differential cross sections measured in terms of the number Y of tritons registering in a triton telescope of solid angle $d\Omega_T$ may be found by solving the equation

$$Y=\int \frac{d\sigma}{d\Omega_T} n dV dF d\Omega_T, \tag{1}$$

where $d\sigma/d\Omega_T$ is the laboratory differential cross section for the $^3\mathrm{He}(\gamma,\pi^+)^3\mathrm{H}$ reaction, n is the number of target nuclei per unit volume, dV is a volume element of the target, and

$$dF=WN(\chi,k)dk/A \tag{2}$$

represents the increment of flux of incident photons. Here W is the total energy content of the irradiation, $N(\chi,k)dk$ is the number of photons between k and $k+dk$ per unit energy in the irradiation for bremsstrahlung of peak energy χ, and A is the cross-sectional area of the beam at the target. Values of $N(\chi,k)$ are obtained from tables of Penfold and Leiss[22] based on the Schiff[23] bremsstrahlung cross section.

Since the coincidence requirement caused some tritons not to be registered when the correlated pion missed the scintillator telescope, the yield Y in our

[16] A. M. Shapiro, Phys. Rev. **84**, 1063 (1951).
[17] R. G. Salukvadze and D. Neagu, Zh. Eksperim. i Teor. Fiz. **41**, 78 (1961) [English transl.: Soviet Phys.—JETP **14**, 59 (1962)].
[18] D. H. Stork, Phys. Rev. **93**, 868 (1954).
[19] V. G. Kirillov-Ugryumov, L. P. Kotenko, E. P. Kuznetsov, F. M. Sergeev, and A. F. Grashin, Zh. Eksperim. i Teor. Fiz. **37**, 1273 (1959) [English transl.: Soviet Phys.—JETP **10**, 907 (1960)].
[20] H. Byfield, J. Kessler, and L. M. Lederman, Phys. Rev. **86**, 17 (1952).
[21] P. P. Kane, Phys. Rev. **112**, 1337 (1958).
[22] A. S. Penfold and J. E. Leiss, Analysis of Photo Cross Sections, Physics Research Laboratory, University of Illinois, 1958 (unpublished).
[23] L. I. Schiff, Phys. Rev. **83**, 252 (1951).

TABLE V. Experimental cross sections.

Telescope settings in lab (degrees) θ_T, θ_π	Kinematically favored pion angle (degrees)	Bin No.	Incident-photon energy in lab (MeV)	Average triton energy in lab (MeV)	Triton lab cross section (μb/sr)	Pion angle in c.m. system (degrees)	Center-of-mass cross section (μb/sr)
26, 111	102	1	182	9.8	17.2±2.3	108	2.55±0.34
	108	2	198	12.5	10.8±1.1	114	1.91±0.20
	111	3	214	15.5	9.8±1.5	117	1.91±0.30
	114	4	230	18.9	6.4±0.8	120	1.35±0.18
	116	5	257	24.5	3.4±0.7	122	0.78±0.16
30, 100	94	1	190	9.7	16.8±2.0	101	2.75±0.32
	99	2	206	12.5	11.6±1.1	106	2.23±0.22
	103	3	224	15.5	11.1±1.8	110	2.33±0.37
	105	4	242	18.5	6.9±1.0	112	1.54±0.22
35, 92.5	82	1	198	9.8	22.8±2.5	88	4.13±0.45
	88	2	217	12.6	13.9±1.2	95	2.94±0.25
	92	3	235	15.5	12.4±1.6	98	2.84±0.37
	94	4	252	18.4	6.7±0.9	100	1.61±0.22
40, 77.5	74	1	216	9.6	16.7±1.5	80	3.56±0.33
	80	2	237	12.4	10.4±0.9	85	2.51±0.22
	82	3	257	15.4	10.1±1.7	89	2.61±0.42

experiment was proportional to an efficiency ϵ so that Eq. (1) becomes

$$Y=\frac{d\sigma}{d\Omega_T}\frac{WnV}{A}\frac{dk}{dE_T}\Delta E_T\frac{S}{(R_c)^2}\epsilon. \tag{3}$$

Here the cross section is assumed slowly varying and is removed from the integral. The variable of integration is changed from k to E_T by the factor dk/dE_T, which is almost linear and varies by $\pm 3\%$ over the included interval of E_T and θ_T. Removing dk/dE_T from the integral and using its value at the center introduces an error of much less than 1%. The factor $S/(R_c)^2$, where R_c is the distance from the target center to the center of the first semiconductor and S is the area of this detector, sets the scale for the solid angle; and ΔE_T is the width of the triton energy bin.

The integrations were carried out in the evaluation of the efficiency

$$\epsilon=\frac{\int N[\chi,k(E_T)](R_c/R)^2 dE_T dV dS}{\int dE_T dV dS} \tag{4}$$

by a 10 000 point Monte Carlo program on a computer. This program selected at random a volume element dV in the target, a surface element dS on the face of the triton detector, and an energy for the triton between the limits of the bin in question. The distance R from dV to dS, the incident photon energy, and the pion energy and angle were then calculated. The pion was tested to see if it struck the scintillator telescope, and the triton was tested to see if it stayed in the telescope until the end of its range. If both answers were affirmative, the event was weighted by $N[\chi,k(E_T)](R_c/R)^2$. Otherwise it was weighted zero. The procedure was repeated in this manner, and the final value of ϵ for that energy bin was the sum of all these weights divided by the number of trials (10 000). Typically, 20–30% of the pions from the trial events hit the pion counter. The average energy of the tritons correlated with observed pions was also calculated for each bin.[11]

An experimental test of the efficiency program and the precision of the angular settings was carried out as follows. With the triton telescope fixed at 35°, data were taken with the pion telescope set at 70°, 81°, 92.5°, 102°, and 111°. The number of experimental pion-triton coincidences should vary with angle in the same way as ϵ, because ϵ was essentially the geometrical-kinematical

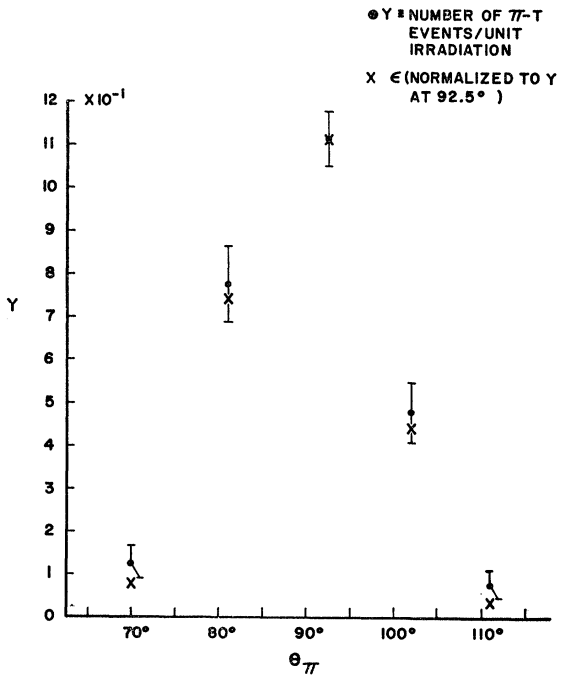

FIG. 8. Comparison of values of ϵ computed by the efficiency program (crosses) with measured yields (circles) as a function of pion telescope angle with the triton telescope fixed at 35°.

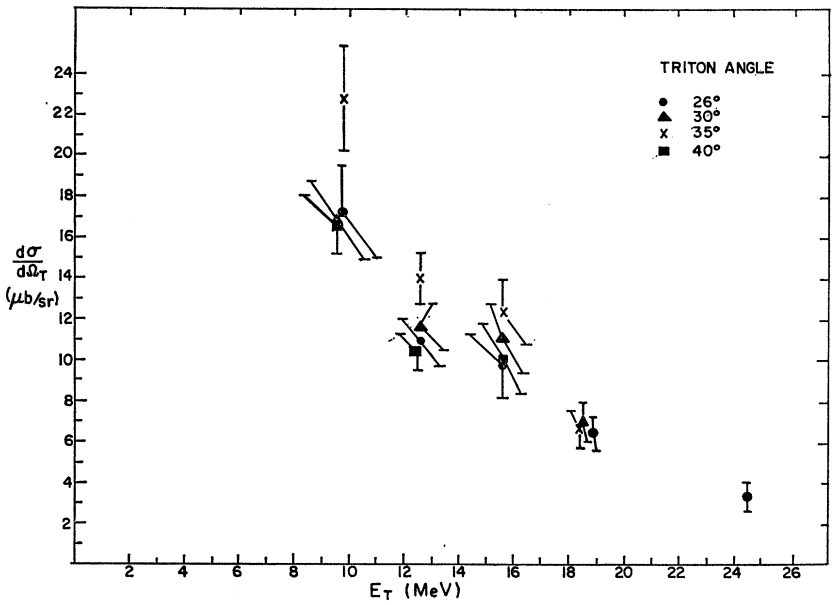

FIG. 9. Absolute differential cross sections in the laboratory system as a function of triton recoil energy. The decrease with increasing energy reflects the overwhelming dependence on momentum transfer.

efficiency of the target-counter system weighted by the bremsstrahlung spectrum. To improve statistics, all triton energies were combined into one bin at each angular setting. The results are plotted in Fig. 8, where ϵ is normalized to the experimental π-T coincidences at 92.5°. The good agreement between ϵ and the experimental points lends confidence to the efficiency calculation.

The calculated values of ϵ were used in Eq. (3) to compute $d\sigma/d\Omega_T$ from the experimental data of Table IV. The results are tabulated in Table V and plotted in Fig. 9, where only statistical uncertainties are shown. Also included in Table V are the cross sections reduced to the center-of-mass system along with various kinematical quantities.

V. INTERPRETATION OF RESULTS

In this section we make a simplified impulse approximation calculation of the reaction $^3\mathrm{He}(\gamma,\pi^+)^3\mathrm{H}$. With some further assumptions about the nature of the nuclear wave functions, we show that this cross section can be directly related to form factors for electron scattering from ^{3}He. The characteristic form factor dependence on momentum transfer is immediately obvious, but the absolute values of our measured cross sections are only 50% to 75% of those calculated. The implications of this discrepancy are discussed.

Apart from kinematic factors, the impulse approximation gives the differential cross section for photopion production from ^{3}He to be proportional to the square of a matrix element

$$T_{fi}\propto\int\exp(-i\mathbf{k}\cdot\mathbf{r}_\pi)\psi_{\mathrm{H}}^*\sum_{j=1}^{3}(\mathbf{A}_j\cdot\boldsymbol{\sigma}_j+B_j)\times\exp(i\boldsymbol{\nu}\cdot\mathbf{r}_\gamma)\psi_{\mathrm{He}}d^3r_\gamma d^3r_\pi d^3r_1 d^3r_2 d^3r_3, \quad (5)$$

where $(\mathbf{r}_1,\mathbf{r}_2,\mathbf{r}_3)$ are the coordinates of the three nucleons; $\boldsymbol{\sigma}_j$ their spins; $\mathbf{r}_\gamma$ and $\mathbf{r}_\pi$ are the photon and pion coordinates; $\mathbf{k}$ and $\boldsymbol{\nu}$ are their momenta; ψ_{H} and ψ_{He} are the ground-state wave functions of ^{3}H and ^{3}He and are functions of the positions, spins, and isospins of the three nucleons. For reasons outlined below, we have neglected final state interactions of the outgoing pion by taking its wave function to be a plane wave. $\mathbf{A}_j\cdot\boldsymbol{\sigma}_j+B_j$ is the most general operator describing photopion production from the jth nucleon. Production is assumed to be at the position of the nucleon, so $\mathbf{A}_j\cdot\boldsymbol{\sigma}_j+B_j$ contains factors of $\delta(\mathbf{r}_\pi-\mathbf{r}_j)$ and $\delta(\mathbf{r}_\gamma-\mathbf{r}_j)$. Therefore the integrals over d^3r_π and d^3r_γ are easily performed. By interchanging pairs of the remaining coordinates and recalling that ψ_{H} and ψ_{He} are both antisymmetric, the three integrals in the sum can be shown to be equal. Finally,

$$T_{fi}\propto 3\int\exp[i(\boldsymbol{\nu}-\mathbf{k})\cdot\mathbf{r}_1]\times\psi_{\mathrm{H}}^*(\mathbf{A}_1\cdot\boldsymbol{\sigma}_1+B_1)\psi_{\mathrm{He}}d^3r_1 d^3r_2 d^3r_3. \quad (6)$$

Explicit assumptions about the nature of the wave functions are necessary for further evaluation. Let each wave function $(\psi_{\mathrm{H}},\psi_{\mathrm{He}})$ be the product of a completely symmetric spatial S state $(U_{\mathrm{H}},U_{\mathrm{He}})$ with spin and isospin states one of which is symmetric and the other antisymmetric.[1,24] Then spin and isospin sums in $T_{fi}{}^2$ may be performed with the result that

$$|T_{fi}|^2\propto(|\mathbf{A}|^2+|B|^2)\times\left|\int\exp[i(\boldsymbol{\nu}-\mathbf{k})\cdot\mathbf{r}_1]U_{\mathrm{H}}^*U_{\mathrm{He}}d^3r_1 d^3r_2 d^3r_3\right|^2. \quad (7)$$

[24] L. I. Schiff, Phys. Rev. 133, B802 (1964).

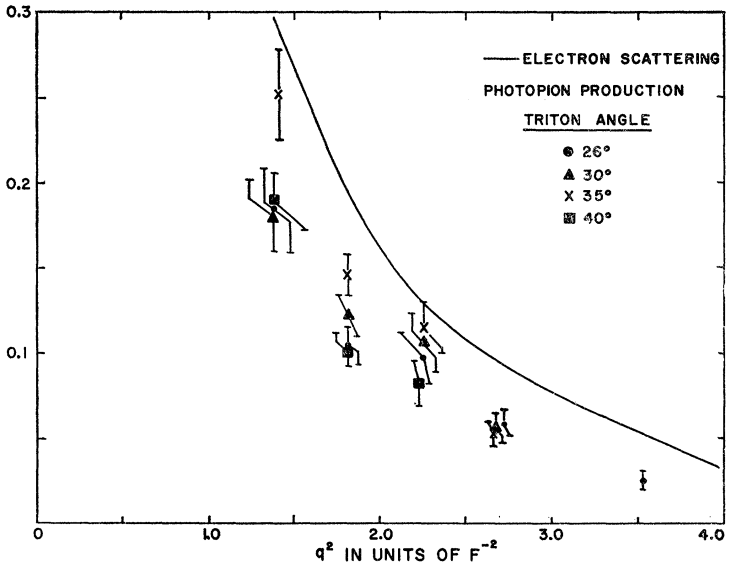

FIG. 10. Test of the validity of the impulse approximation and other assumptions made in the analysis. The smooth curve was drawn through values of the square of the matter form factor obtained from electron scattering experiments. The experimental points represent the ratio R_1 of our measured cross sections to free-proton cross sections with appropriate flux factors.

In Eq. (7) the terms $|\mathbf{A}|^2$ and $|B|^2$ contain momentum and kinematic factors which should, in principle, be retained in the integral. In removing these factors from the integral we have assumed that the nuclear momenta are not large enough to affect them materially.

After spin and isospin sums are performed, the coefficient of $|\mathbf{A}|^2$ is 1. This reflects the fact that of the two protons available, only one can be turned into a neutron with its spin flipped and still satisfy the Pauli principle with the other neutron remaining in ^3H. Similarly, $|B|^2$ also has the coefficient 1 because only one proton (the "other" one) can be changed into a neutron without spin flip. Since $|\mathbf{A}|^2+|B|^2$ is the same dynamic factor that occurs for π^+ photoproduction from a proton, the cross section in the center-of-mass system may be derived from the matrix element of Eq. (7) as[25]

$$d\sigma/d\Omega(^3\mathrm{He})=\Phi d\sigma/d\Omega(p)\,|F(q^2)|^2, \tag{8}$$

where

$$\Phi=[W^2/kE_pE_\pi E_n]_p[kE_{\mathrm{He}}E_\pi E_{\mathrm{H}}/W^2]_{\mathrm{He}}, \tag{9}$$

and

$$F(q^2)=\int \exp i\mathbf{q}\cdot\mathbf{r}_1 U_{\mathrm{H}}^* U_{\mathrm{He}} d^3r_1 d^3r_2 d^3r_3, \tag{10}$$

with $\mathbf{q}=\mathbf{v}-\mathbf{k}$. $d\sigma/d\Omega(p)$ is the cross section for photoproduction from a free proton. The ratio Φ contains kinematic factors which arise in the evaluation of the cross sections from the matrix elements. Numerically, Φ is nearly constant, varying from 1.63 to 1.70 over the range of energies studied in this experiment. W is the total energy; $\mathbf{k}$ is the meson momentum; E_p, E_n, E_{He}, E_{H}, and E_π are the total energies, respectively, of the proton, neutron, ^3He, ^3H, and pion. The quantities in the first bracket of Φ are to be evaluated in the center-of-mass system of a photon and a free proton; those in the second bracket in the center of mass of a photon-^3He system. The factors in the first bracket of Φ have been removed from the integral under the same assumption as the photoproduction operator. The overlap integral $F(q^2)$ is a function of the square of the momentum transferred to the triton, which, for energies considered here, is proportional to triton kinetic energy. If the ^3H and ^3He ground state wave functions are identical, then $F(q^2)$ is the nuclear matter form factor for ^3H or ^3He.

In Fig. 10 we have plotted the ratio R of our measured center-of-mass cross sections to $\Phi d\sigma/d\Omega(p)$. If the simple theory presented above were correct, this would be a graph of the square of the matter form factor versus the square of the momentum transfer. For comparison, therefore, we have plotted on the same graph the square of the matter form factor derived from electron-scattering measurements. Although it is clear that there is a general agreement between the simple theory and experiment, our points lie from 25% to 50% low, indicating a smaller cross section than that predicted. Notice that after the free proton cross section has been divided out, no explicit dependence on the angle remains which is outside statistical error, although the points at 35° triton angle lie suspiciously high. It may also be worth noting that the entire disagreement disappears if $\Phi=1$, the approximation of infinitely heavy nuclear mass.

In plotting Fig. 10, values for $d\sigma/d\Omega(p)$ were calculated from the theory of Chew, Goldberger, Low, and Nambu[26] as tabulated by Robinson.[27] Some ambiguity

[25] This same expression has been derived by more general methods by V. V. Balashov, G. Ya. Korenman, and T. S. Macharadze, J. Nucl. Phys. (USSR) 1, 668 (1965).

[26] G. Chew, M. Goldberger, F. Low, and Y. Nambu, Phys. Rev. 106, 1345 (1957).

[27] C. S. Robinson, Technical Report No. 8, Contract ONR 1834(05), Physics Research Laboratory, University of Illinois, 1963 (unpublished).

TABLE VI. Comparison with free nucleon production.

Triton angle, lab system (degrees)	Photon energy in lab (MeV)	$\frac{d\sigma}{d\Omega}(^3\mathrm{He})$ c.m. system μb/sr	$\frac{d\sigma}{d\Omega}(p)_1$ c.m. system μb/sr	$\frac{d\sigma}{d\Omega}(p)_2$ c.m. system μb/sr	q^2	Values for the ratio R obtained from the measured cross sections R_1	R_2
26	182	2.55±0.34	8.4	10.3	1.4	0.184 ±0.025	0.200 ±0.027
30	190	2.75±0.32	9.3	10.9		0.181 ±0.021	0.201 ±0.024
35	198	4.13±0.45	10.1	12.2		0.252 ±0.027	0.266 ±0.029
40	216	3.56±0.33	11.5	13.0		0.189 ±0.017	0.211 ±0.019
26	198	1.91±0.20	10.3	12.6	1.8	0.113 ±0.011	0.123 ±0.013
30	206	2.23±0.22	11.2	13.6		0.122 ±0.012	0.128 ±0.013
35	217	2.94±0.25	12.3	15.8		0.146 ±0.012	0.144 ±0.012
40	237	2.51±0.22	14.6	17.6		0.103 ±0.009	0.109 ±0.009
26	214	1.91±0.30	12.0	15.3	2.2	0.097 ±0.015	0.097 ±0.015
30	224	2.33±0.37	13.3	16.9		0.106 ±0.017	0.106 ±0.017
35	235	2.84±0.37	14.9	19.9		0.115 ±0.015	0.111 ±0.014
40	257	2.61±0.42	18.7	22.3		0.082 ±0.013	0.088 ±0.014
26	230	1.35±0.18	13.9	19.0	2.7	0.0585±0.0076	0.0546±0.0071
30	242	1.54±0.22	15.8	21.3		0.0583±0.0082	0.0553±0.0079
35	252	1.61±0.22	17.8	23.5		0.0535±0.0073	0.0517±0.0070
26	257	0.78±0.16	17.6	24.1	3.5	0.0259±0.0054	0.0242±0.0051

exists about the energies and angles at which to compute $d\sigma/d\Omega(p)$ and Φ. We have measured $d\sigma/d\Omega(\mathrm{He})$ for definite values of the ^{3}H recoil energy and angle, which unambiguously determine the photon energy and the pion energy and angle. The problem is that for the same photon energy incident on a free proton and for the same pion angle, the pion energy is different. In plotting Fig. 10, we have chosen to evaluate $\Phi d\sigma/d\Omega(p)$ for the same *photon energy in the laboratory and the same magnitude of momentum transfer.*

The ratio R_1 of our measured cross sections to Φ $d\sigma/d\Omega(p)$ calculated in this way are tabulated in Table VI and have been used to plot the experimental points in Fig. 10. We have also calculated $\Phi d\sigma/d\Omega(p)$ for the case of equal *vector* momentum transfer. The resulting values for R are tabulated as R_2 in Table VI. The difference in these assumptions is appreciable, but in no case exceeds our statistical errors.

Under the assumption that the ^{3}H and ^{3}He wave functions are the same, Schiff[24] shows that the nuclear matter form factor F_B is related to charge form factors by

$$F_B=\frac{2F_{\mathrm{ch}}(^3\mathrm{He})+F_{\mathrm{ch}}(^3\mathrm{H})}{3[F_{\mathrm{ch}}(p)+F_{\mathrm{ch}}(n)]}. \qquad (11)$$

Since the charge form factors $F_{\mathrm{ch}}(^3\mathrm{He})$ and $F_{\mathrm{ch}}(^3\mathrm{H})$ have been measured by Collard *et al.*[2-4] and $F_{\mathrm{ch}}(p)$ and $F_{\mathrm{ch}}(n)$ are known, F_B can be found. The curve in Fig. 10 was plotted from F_B computed in this way by Srivastava.[28]

We may search for the discrepancy between the results of this experiment and the predictions of the simple theory in three principal places: (1) the assumptions made about the nuclear wave functions of ^{3}H and ^{3}He; (2) the assumption of a plane wave for the wave function of the outgoing pion; (3) the assumption in the impulse approximation that the amplitudes for production from bound nucleons are the same as those from free nucleons.

Except for negligible Coulomb and neutron-proton mass-difference effects, charge independence of nuclear forces requires that ^{3}H and ^{3}He have the same nuclear wave function, and, therefore, that the assumptions made in Eq. (11) are likely quite justified. The electron scattering measurements[2-4] indicate a difference in the charge form factors of ^{3}H and ^{3}He which is difficult to understand unless the ground state is not completely symmetric. The assumptions leading from Eq. (6) to Eq. (7) are, therefore, not completely justified and there is no such simple relation between the electron scattering and pion photoproduction as indicated by Eq. (8). Just what the correct relation should be must await more detailed calculation, but we think it unlikely that any reasonable wave function would explain both our results and the electron scattering results.

Recently, Theuss *et al.*[29] have found it necessary to give a smaller *nuclear matter* radius to ^{3}H than to ^{3}He in order to explain their *d-d* scattering results. If we calculate $R=|F(q^2)|^2$ from Eq. (10) using Gunn and Irving[30] wave functions of the form

$$U=N\exp[-\mu(\sum_{i>j}^{3} r_{ij}^2)^{1/2}]/(\sum_{i>j}^{3} r_{ij}^2)^{1/2}, \qquad (12)$$

with the size parameter $1/\mu_{\mathrm{He}}=2.6F$ (a value consistent with the photodisintegration value of Berman *et al.*[31])

[28] B. K. Srivastava, Phys. Rev. 133, B545 (1964).

[29] R. B. Theus, W. I. McGarry, and L. A. Beach, Phys. Rev. Letters 14, 232 (1965).

[30] J. C. Gunn and J. Irving, Phil. Mag. 42, 1353 (1951).

[31] B. L. Berman, L. J. Koester, and J. H. Smith, Phys. Rev. 133, B117 (1964).

and $1/\mu_H = 2.3F$ (a value consistent with Theuss[28]), we find that the integral in Eq. (9) is reduced at small momentum transfers but increased at the momentum transfers of this experiment. The agreement with our data is made considerably worse.

At pion energies below 90 MeV with which we are concerned, nuclear absorption of the outgoing pion is unlikely to be as large as the discrepancies found here. For example, a naive mean-free-path argument shows that, on the average, only about 13% of the pions would be absorbed. The effects of nonabsorptive distortion of the plane waves used in our simple calculation are more difficult to understand, and their evaluation must await a more careful calculation.

Finally we come to the question of whether the pion production itself is suppressed in nuclear matter. Such a suppression of charged pion production in complex nuclei below that expected from free nucleons has been observed many times in the past and has been referred to by some as the $A^{2/3}$ law.[32] In these charged pion production experiments the final state conditions have always been less well defined than in the present experiment and therefore subject to other interpretations.

Several experimenters have observed neutral pion photoproduction in which the final state remains bound. Friedman and Kendall[33] found a suppression of elastic π^0 photoproduction in deuterium near 300 MeV whereas at higher energies their results agreed more nearly with a form-factor calculation. They attributed this suppression to multiple-scattering effects in deuterium.[34] Belousov *et al.*[35] observed that π^0 production from deuterium near 200 MeV decreased too rapidly at angles greater than 90° to be explained by a form factor. Palit and Bellamy[36] have seen a similar suppression in π^0 photoproduction from ^4He. On the other hand, for energies very close to threshold, Schrack, Penner, and Leiss[37] find no such suppression from heavier elements.

Suppression of pion production in nuclear matter has been variously ascribed to multiple-scattering corrections or to self-absorption of the pions with production of quasideuteron photodisintegration as in the Wilson model.[38,39] We are inclined to think that the discrepancy between the simple impulse approximation calculation and our results comes from some such effect, but our accuracies are not great enough to warrant any detailed comparison with those theories.

VI. SUMMARY

We have measured the cross section for the reaction $^3He(\gamma,\pi^+)^3H$ over a range of energies and angles. We find that the cross section is grossly described by the cross section from a single free proton times the square of the nuclear matter form factor for ^3He, modified by kinematic factors. The cross section is therefore primarily a function of the recoil triton energy, with additional variations in energy and angle only through the rather weak dependence of the free-proton cross section.

In detail, however, the cross section lies from 25 to 50% below the simple form-factor theory. This discrepancy may arise from the use of insufficiently accurate wave functions in the simple theory, but it is more likely due to a suppression of pion production in nuclear matter.

ACKNOWLEDGMENTS

The authors would like to thank Professor D. G. Ravenhall and Professor Roy Schult for advice concerning theoretical aspects of this work. We are grateful to Lee Rogers, Don Vermillion, and the betatron staff for their aid in setting up and running the experiment; to Ed Garrison for help with cryogenic problems; and to Mrs. Nancy O'Fallon, Dennis Herzo, and Charles Stenberg for assistance in data-taking.

[32] See, for example, R. M. Littauer and D. Walker, Phys. Rev. **86**, 838 (1952).
[33] J. I. Friedman and H. W. Kendall, Phys. Rev. **129**, 2802 (1963).
[34] J. Chappelaer, Phys. Rev. **99**, 254 (1955).
[35] A. S. Belousov, A. I. Lebedev, S. V. Rusakov, E. I. Tamm, L. S. Tatarinskaya (private communication from E. I. Tamm).
[36] P. Palit and E. H. Bellamy, Proc. Phys. Soc. (London) **72**, 880 (1958).
[37] R. A. Schrack, S. Penner, and J. E. Leiss, Phys. Rev. **127**, 1772 (1962).
[38] R. R. Wilson, Phys. Rev. **104**, 218 (1956).
[39] A. S. Belousov, B. B. Govorkov, and V. I. Gol'danskii, Zh. Eksperim. i Teor. Fiz. **36**, 244 (1959) [English transl.: Soviet Phys.—JETP **9**, 164 (1959)].